RSC Advances

PAPER

View Article Online
View Journal | View Issue

Cite this: *RSC Adv.*, 2016, **6**, 2270

Toward bandgap tunable graphene oxide nanoribbons by plasma-assisted reduction and defect restoration at low temperature

Wei-Hung Chiang,[a] Ting-Chun Lin,[b] Yan-Sheng Li,[a] Yu-Jhe Yang[c] and Zingway Pei*[bc]

Received 16th October 2015
Accepted 22nd December 2015

DOI: 10.1039/c5ra21537d

www.rsc.org/advances

Simultaneous reduction and defect restoration of graphene oxide nanoribbon (GONR) *via* plasma-assisted chemistry is demonstrated. Hydrogen (H_2) and methane (CH_4) gases are continuously dissociated in a plasma to produce atomic hydrogen and carbon-containing ions and radicals carried by the gas flow to react with and remove oxygen functional groups from GONR films. Detailed material characterization confirms that the synergistic effect of simultaneous reduction and defect restoration of GONR occurred during the H_2/CH_4 plasma treatment. Extensive optical transmittance measurement suggests that the optical energy gap of the as-treated reduced GONR (r-GONR) can be engineered by controlling the plasma exposure time. Systematic electrical measurement indicates that the electrical conductivity of as-treated r-GONR can be enhanced after H_2/CH_4-plasma treatment. The unique H_2/CH_4-plasma reduction with characteristics of short process time, high purity, and low temperature compared with conventional thermal and chemical reductions suggests that this nonequilibrium chemical approach can be used for industrial-scale reduction of GONR and graphene oxide (GO).

Introduction

Graphene nanoribbon (GNR) and reduced graphene oxide nanoribbon (r-GONR) represent unique forms of graphene and have spurred intensive interests due to their exceptional physical and chemical properties[1] for emerging applications such as energy generation and storage,[2,3] chemical and biosensors,[4,5] catalysis,[6] nanocomposites,[7] and nanoelectronics.[8] Many methods have been proposed to produce GNR including longitudinal unzipping of carbon nanotubes (CNTs),[9] plasma etching,[10] metal catalyst assisted cutting,[11] lithium insertion and exfoliation,[12] and mechanical sonication in organic solvents.[13] Among those methods, the reduction of graphene oxide nanoribbon (GONR) is a promising alternative for bulk production of GNR-based materials as it can be synthesized in large quantities from longitudinal unzipping of CNTs and solubilized in a variety of solvents.[14] Consequently the development of controllable reduction of GONR is attractive for both fundamental study and innovative applications.

One of the critical challenges for technological applications of GONR is the presence of oxygen functional groups that must be controlled to precisely tune their electronic and optical properties. Several methods have been reported to reduce the GONR or graphene oxide (GO) including chemical reduction by chemical agents such as hydrazine (N_2H_4)[15,16] or sodium borohydride ($NaBH_4$).[17] Treatment of GONR with those chemicals, however, is time-consuming, laborious, and generally ineffective, requiring extra high temperature (usually above 1000 °C) annealing steps.[18] Moreover hydrazine is not easy to handle, environmentally toxic, and can introduce impurities in the reduced GO. Thermal annealing in Ar, H_2, or ultrahigh vacuum (UHV) environments has been found to remove oxygen effectively.[19,20] However, the high temperature condition limits the range of substrates. Therefore, it is still required to develop a low-temperature, facile, and green approaches to reduce GONR. Compared with other chemical methods, plasma technology offers an unique advantage because nonequilibrium reactions can be performed at low temperature and high purity.[21] In the case of GONR, the generation of atomic hydrogen from H_2 plasma could enable effective removal of oxygen functional groups.[18] However, plasmas contain energetic species such as ions that can bombard and sputter or damage such atomically thin materials.[22] The defects result from the reduction may affect the graphene quality. Consequently, GONR reduction and defect repair have become crucial issues. Recent studies have demonstrated that the CH_4-related plasmas can be used to reduce and repair defects in GO by the CH_n^+ ions and CH_n free radicals generated in the plasma.[23,24] However, little has been systematically reported on the effect of CH_4-related plasmas on the reduction level and structure change of GONR. Moreover the relationship between the optical and electrical properties of r-

[a]*Department of Chemical Engineering, National Taiwan University of Science and Technology, Taipei 10607, Taiwan*

[b]*Department of Electrical Engineering, National Chung Hsing University, Taichung 402, Taiwan. E-mail: zingway@dragon.nchu.edu.tw*

[c]*Graduate Institute of Optoelectronic Engineering, National Chung Hsing University, Taichung 402, Taiwan*

GONR treated by CH_4-related plasmas and the plasma parameters is still not clear. Overall, there are several advantages of plasma-assisted reduction of GONR. First of all, it is possible to directly reduce the GONR on thermal-sensitive substrates such as polymeric materials due to the lower process temperature in a plasma-assisted reduction. Secondary, defect restoration of GONR can be achieved under CH_4-containing plasma, making the materials property of as-treated r-GONR further improved.

Here we report an effective and controllable method to simultaneously reduce the oxygen-containing functionalities and defect repairing of GONR using a H_2/CH_4-plasma treatment at low temperature of 240 °C. The process temperature in our work is much lower than that of conventional thermal reduction method (usually above 1000 °C),[18] making it is promising to directly reduce the GONR on thermal-sensitive substrates such as polymeric materials. Hydrogen and methane gases are continuously dissociated in plasma to produce atomic hydrogen and carbon-containing radicals carried by the gas flow to react with and remove oxygen functional groups from GONR films *via* radical-assisted chemistry. The main reason for using these two gases was that the ions (H^+, CH_n^+ $n = 1$–5 and C^+) and free radicals (*i.e.*, H and CH_n) in the plasma, and neutral gas (H_2) that collided on the thin-film surface are easily absorbed, which react with oxygen and generate products (CO, OH, and H_2O).[24] In particular, H_2/CH_4- plasma treatment showed more effective in GONR reduction than CH_4-plasma treatment. Extensive materials characterizations including Fourier transform infrared (FTIR) spectroscopy, X-ray photoelectron spectroscopy (XPS), and micro Raman spectroscopy indicate that GONR can be reduced and density of sp^2 graphene domain was increased using a H_2/CH_4-plasma treatment. Optical transmittance measurement shows that the optical energy gap of the as-treated reduced GONR (r-GONR) can be tuned by simply controlling the plasma exposure time. Systematic electrical measurement indicates that the electrical conductivity of as-treated r-GONR can be enhanced after H_2/CH_4-plasma treatment. The unique H_2/CH_4-plasma reduction with characteristics of short process time, high purity, and low temperature compared with conventional thermal reduction suggests that this nonequilibrium chemical approach can be used for industrial-scale reduction of GONR as well as GO.

Experimental

Chemicals

Potassium permanganate ($KMnO_4$, 98%), hydrogen peroxide (H_2O_2, 35%), and ether [$(C_2H_5)_2O$, 99+%] were purchased from ACROS. Potassium nitrate (KNO_3, 95%) was obtained from JT-Baker. Sulfuric acid (H_2SO_4, >95%) and hydrochloric acid (HCl, 37%) were purchased from Scharlau. All the chemicals were used without any further purification.

GONR synthesis

The CNTs used in the present study were multi-walled CNTs (MWCNTs) synthesized using a catalytic chemical vapor deposition (CVD). Details of the CNT growth process were similar to that previously described.[25] In a typical preparation, 0.1 g of MWCNTs was suspended in a different amount of concentrated H_2SO_4 and 1 g KNO_3 and then stirred at 300 rpm for 2 h using a magnetic stirrer until a visually homogeneous black solution formed. Details of the GONR synthesis were similar to that previously described.[2] Then 0.5 g $KMnO_4$ was slowly added to the solution and further stirred for 2 h at room temperature. After that, the temperature was gradually raised to 70 °C and maintained at that temperature for 2 h in water bath (IKA-HS7 digital). When the reaction was completed, the product was purified and dried with a series steps reported elsewhere.[26] Briefly, each mixtures were removed from the heat source, allowed to cool to room temperature and poured into 350 g of ice containing 5 mL of 35% H_2O_2 (to prevent precipitation of insoluble MnO_2). The mixtures were then centrifuged (24 500 rpm, 30 min) to give crude GNRs solid (Beckman, Avanti J-25). The solid was removed and then bath-sonicated in 60 mL deionized (DI) water for 30 min (IKA-HS7 digital). The material was bath-sonicated again by adding 30 mL HCl, and then the dispersion was centrifuged (24 500 rpm, 30 min). Furthermore, the collected solid was removed and then bath-sonicated in 60 mL ether for 30 min. In the end, the purified GONRs were obtained by collecting the centrifuged (24 500 rpm, 30 min) solid.

Plasma reduction

The GONR solution was prepared by dissolving the GONRs in deionized water (0.025 wt%). The GONR solution was oscillated in an ultrasonic oscillator for 30 min to homogenize the GONR solution and facilitate subsequent coating on basal plates. Next, 0.5 mL of the oscillated GONR solution was applied to drop-casted glass and silicon basal plates as a coating. The coatings of GONR thin films then underwent plasma-enhanced chemical vapor deposition for plasma processing. The reactor for plasma reduction was made by a stainless steel (SUS 316) equipped with a radio-frequency (rf, 13.56 MHz) power generator (Advanced Energy) and a load-lock system. The plasma was generated in the parallel plate configuration in which bottom plate was used as the sample susceptor and heater while the upper plate was used to feed the rf power. The rf power was conducted into the system with negligible reflectance by a matching box. The diameter for plates is 10 cm and the distance between two plates is 5 cm. The gas inlet was controlled by mass flow controller (MFC) in the unit of standard mL min^{-1} (sccm). A dry pump/turbo pump combination was used to pump the pressure of the chamber to high vacuum. And the process pressure of the chamber was controlled by a butterfly valve. Prior to plasma treatment, the react chamber is pumping down to 1×10^{-6} Torr. After sample loading, the substrate was heated to 240 °C. The reduction gas, CH_4, in 100 sccm was conducted into reaction chamber. The process pressure is 400 mTorr controlled by butterfly valve. The rf power of 100 W was then performed on the sample for 5, 10, 15 and 30 min. The parameters for processing $H_2 + CH_4$ plasma included an H_2 and CH_4 gas mixture flow of 100 sccm, with all other parameters the same as that for CH_4 plasma.

Characterization

The SEM images of raw MWCNTs and as-synthesized GONRs were performed on JEOL JSM-6500F (accelerating voltage = 15 kV). Samples were prepared by pressing powders on the copper tape. The transmission electron microscopy (TEM) images of raw MWCNTs and as produced GONR were collected on Hitachi H-9500. Samples were prepared by dispersing raw MWCNTs and as-synthesized samples in ethanol and then drop onto 300 mesh holey lacy carbon grids on cupper support (Ted Pella, Inc.) at ambient condition. The GONR and r-GONR thin films were fabricated on silicon basal plates were analyzed using FTIR (Nicolet Magna-IRIM 550), XPS (Ulvac Phi PHI 5000), and Raman spectroscopy (NT-MDT, $\lambda = 532$ nm). The purpose of these analyses was to determine the element content, chemical bonding, and molecular structure variations before and after reduction. The GONR thin films fabricated on glass basal plates were measured using UV-Vis (Hitachi U-3010) to obtain the transmittance. The acquired transmittance and the average thickness measured using the step method were used to calculate the absorption coefficient and optical bandgap. Thin films fabricated on glass basal plates were used to coat aluminum (Al) electrodes through thermal evaporation. The Agilent B2912A measuring system was employed to measure the electric current and voltage of the components to identify the differences in the electrical properties of the current–voltage (I–V) curve. The sheet resistance and electrical conductivity were then calculated.

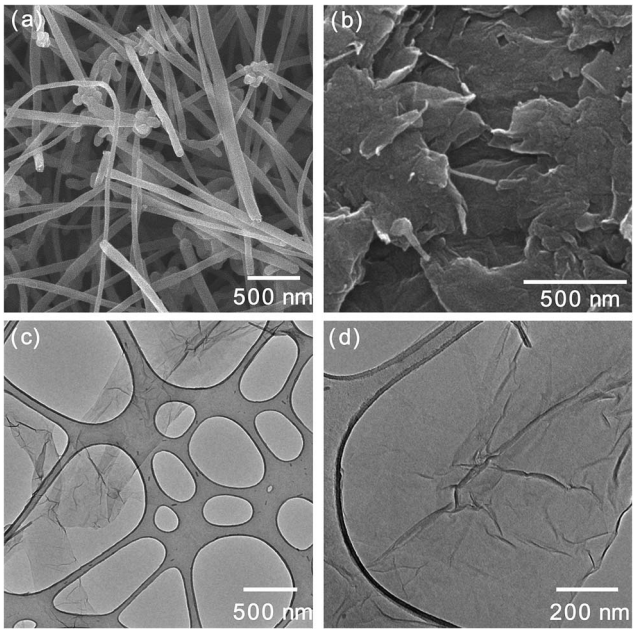

Fig. 1 The SEM micrographs of (a) pristine MWCNTs and (b) as-produced GONR. (c) The TEM and (d) HRTEM image of as-produced GONR.

Results and discussion

The morphology of as-produced GONR by CNT unzipping can be directly observed by electronic microscope. Fig. 1(a) shows the SEM micrograph of starting MWCNTs with the diameters

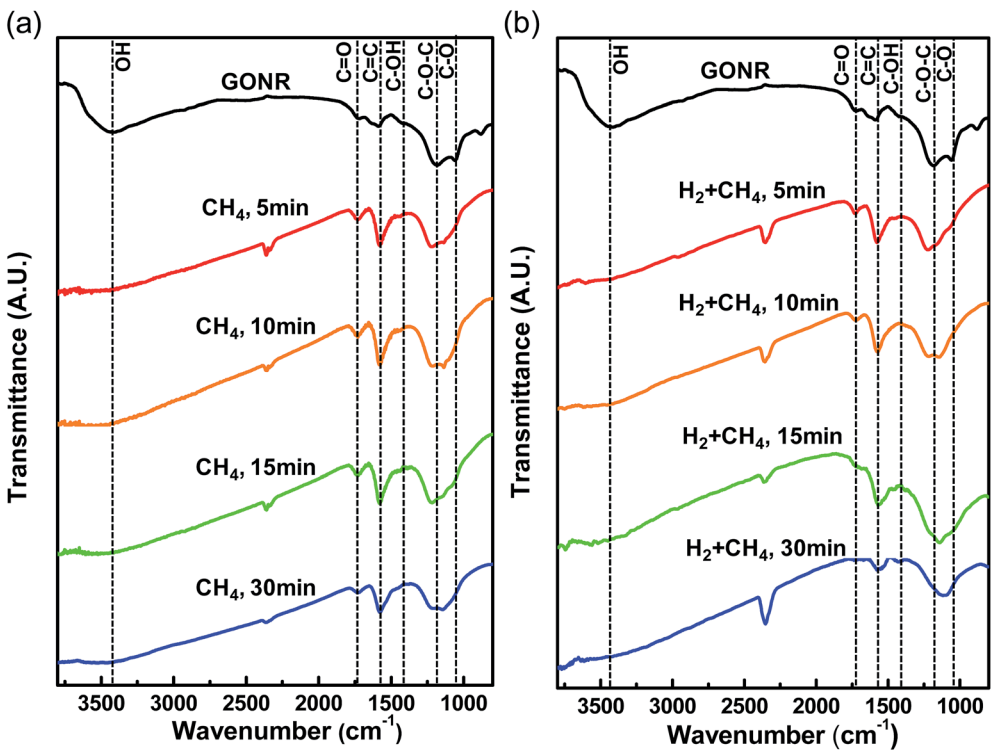

Fig. 2 FTIR spectra of (a) starting GONR and r-GONRs treated with CH_4-plasma with 5, 10, 15, and 30 minutes and (b) starting GONR and r-GONRs treated with H_2/CH_4-plasma with 5, 10, 15, and 30 minutes.

varying from 50 to 100 nm and lengths ranging from 8 to 10 μm. As compared to the pristine CNT, we can see that most of the as-produced GONR possesses unzipped structures after chemical oxidation [Fig. 1(b)]. This result is also supported by TEM image of as-produced products [Fig. 1(c) and (d)], where the tubular structure of nanotubes cannot be observed in the as-produced product instead of the appearance of unzipped layer structure.

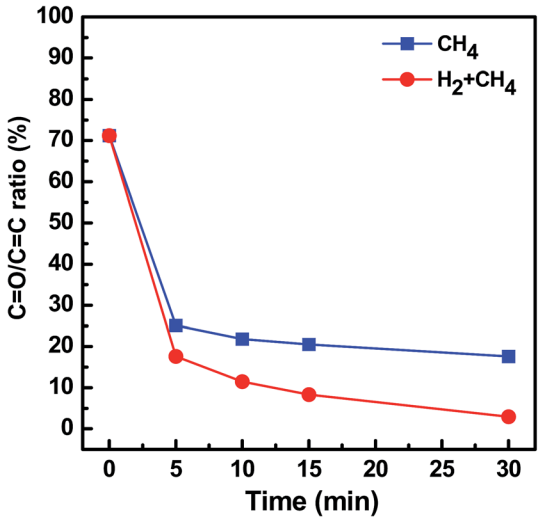

Fig. 3 Plot of C=O/C=C ratio estimated from the FTIR spectra of GONRs treated with CH_4- and H_2/CH_4-plasmas as a function of plasma treatment time.

Our result is in agreed with previous study.[9,27] In addition, very thin layers were obtained [Fig. 1(d)] in the high-resolution TEM (HRTEM) observation, and most of nanotubes were cut and unzipped into small pieces as shown in SEM image [Fig. 1(a)]. On the basis of the SEM and TEM observation, we demonstrated a simple solution-based oxidative process to produce GONR by lengthwise cutting and unraveling of MWCNT side walls, and the as-produced GONR can be used to study the effect of plasma-assisted reduction.

FTIR spectroscopy was used to characterize the functional groups of starting GONR and as-treated r-GONRs by CH_4 and H_2/CH_4 plasmas, and the spectra are shown in Fig. 2. The spectrum of starting GONR [Fig. 2(a)] exhibits several peaks including sp^2 graphitic C=C stretching, C–OH stretching, C–O–C epoxy asymmetric stretching, C=O carbonyl and C–O epoxy stretching of COOH carboxyl group, at 1585, 1420, 1420, 1730, 1058 cm^{-1}, respectively.[9,28,29] The result indicates that the starting GONR composes the oxidized graphene structure, which is consistent with previous work.[9,27] After 5 min CH_4- or H_2/CH_4-plasma treatments, the intensities of oxygen functional groups of the as-treated samples were largely decreased [Fig. 2(a) and (b)], suggesting that the oxygen functional groups on the GONR surface were effectively reduced by plasma exposure. In addition, the peak intensity of C=C stretching was found to be increased substantially after 5 min CH_4- and H_2/CH_4-plasma treatments, implying that the transformation of sp^3 carbon bonding to sp^2 graphene domain was occurred

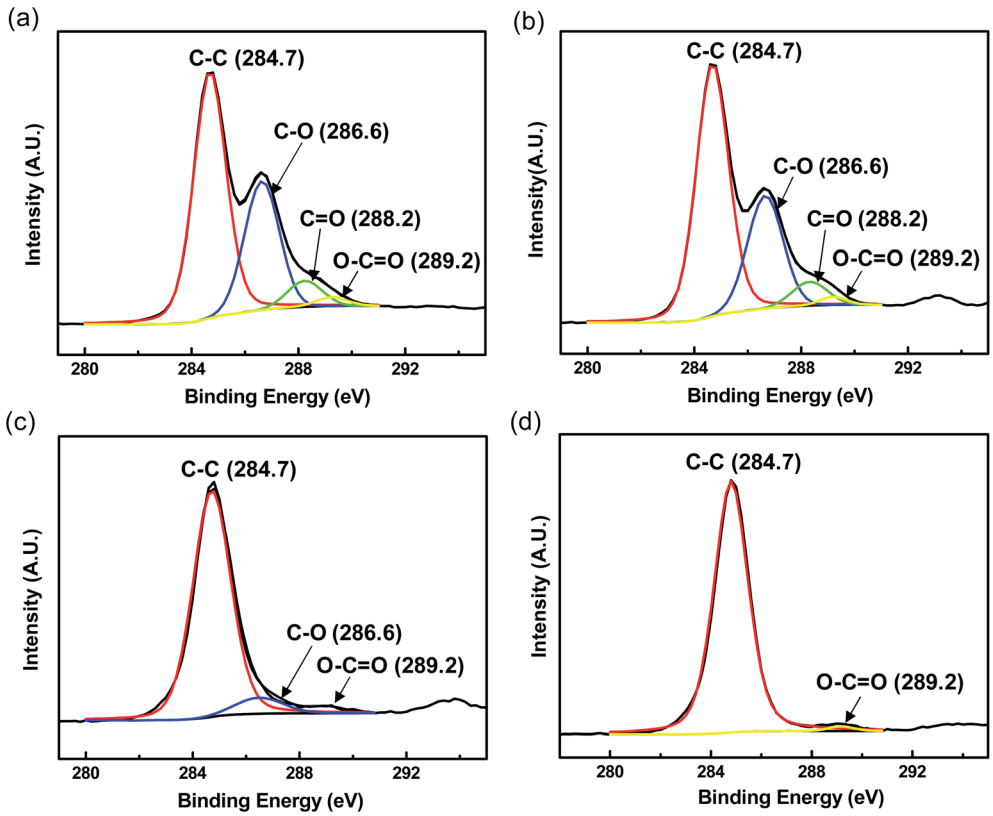

Fig. 4 XPS C 1s core level spectra of (a) starting GONR, and r-GONRs treated by H_2/CH_4-plasma with (b) 5, (c) 10, and (d) 30 minutes.

Table 1 XPS analysis of atomic percentages (atom%) of different carbon bonds in the as-treated r-GONR films treated with different plasma exposure time

Time (min)	C–C (atom%)	C–O (atom%)	C=O (atom%)	COOH (atom%)
0	61.2	28.6	7.1	3.1
5	62.9	27.6	7	2.5
10	90.2	8.3	<1	1.2
30	98.5	<1	<1	1.2

during the treatment.[23] The peak intensities of the oxygen functional groups on the GONR were found to be gradually decreased while those of the C=C stretching were increased with the increased treatment time from 5 to 30 min under CH_4- and H_2/CH_4-plasma treatments. To further reveal the treatment time effect on the reduction level of GONR, an empirical quantitative analysis was performed by calculating the ratio of C=O and C=C peaks (C=O/C=C) in the FTIR spectra to emphasize the level of oxidation in the C=C matrix.[30] Fig. 3 shows the plot of C=O/C=C ratio as a function of treatment time. It is indicated that the C=O/C=C ratios were significantly decreased from 71.2% to 25.1% and 17.6% with 5 min CH_4- and H_2/CH_4-plasma treatments, respectively, and contentiously decreased to 17.6% and 2.9% after 30 min CH_4- and H_2/CH_4-plasma treatments, respectively. The result suggests that the reduction level and defect repairing of GONR can be controlled by adjusting the plasma exposure time. Moreover, it turns out that H_2/CH_4-plasma is more effective than CH_4-plasma in terms of the efficiency of reduction and defect repairing of GONR (Fig. 3).

XPS was performed to further study the surface functionalities of the starting GONR and as-treated r-GONR by H_2/CH_4-plasma with varying treatment time, and the result was shown in Fig. 4. Fig. 4(a) shows the XPS C 1s core level spectrum of the starting GONR and, four peaks were indicated including sp^2 C–C, C–O, C=O, and O–C=O at 284.7 eV, 286.6 eV, 288.2 eV, and 289.2 eV, respectively.[9,24] These assignments are consistent with previous reports of GO and GONR.[9,24] The XPS quantification result is summarized in Table 1. As the H_2/CH_4-plasma treatment time was increased, the peaks corresponding to C–O (286.6 eV), C=O (288.2 eV), and O–C=O (289.2 eV) were continuously reduced [see Fig. 4(b)–(d)], which is in consistent with the FTIR analysis (Fig. 2 and 3). The H_2/CH_4-plasma assisted reduction was found not only efficient on the reduction C–O bonding, the majority of oxygen species in the starting GONR reduction, but also the C=O and O–C=O species [Fig. 4(c) and (d)] that have been found to decorate the edges of GONR sheets and are believed to be more difficult to remove.[31] After 30 min H_2/CH_4-plasma treatment, the oxygen functionalities were almost removed except a small portion (1.2 atom%) of O–C=O (289.2 eV) in the as-treated r-GONR, showing the effectiveness of reduction of GONR using the H_2/CH_4-plasma treatment.

Additional atomic-scale structural changes to the GONR as a result of plasma treatment were evaluated by micro Raman spectroscopy. Fig. 5 shows a series of Raman spectra obtained for starting GONR and r-GONR treated by CH_4- and H_2/CH_4-plasmas

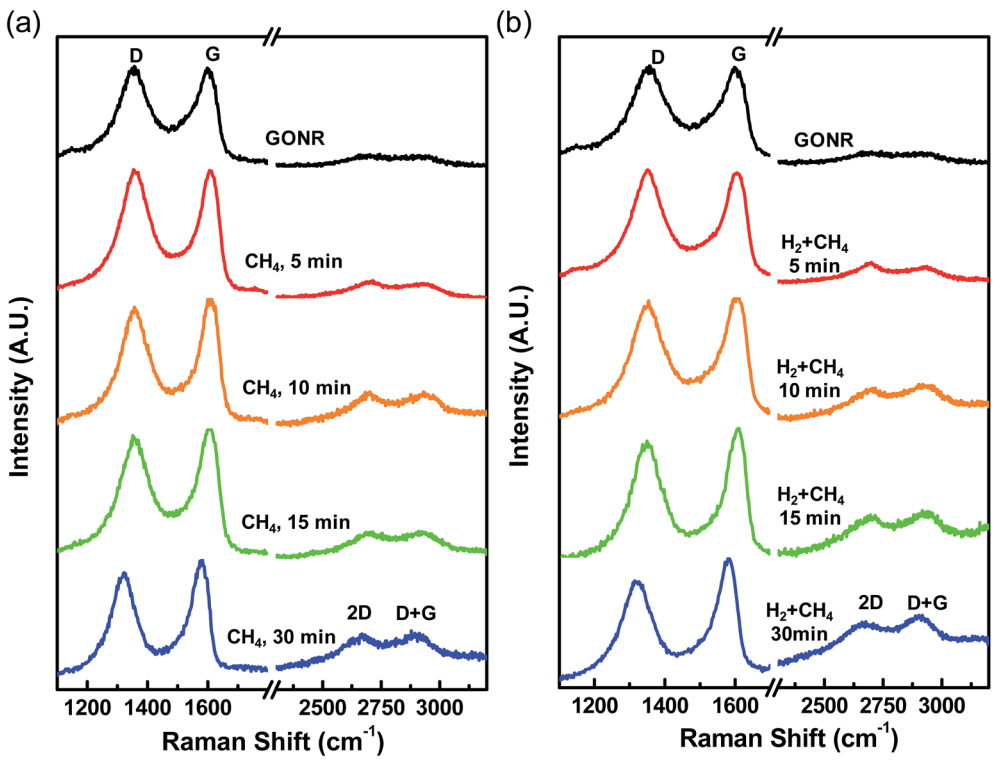

Fig. 5 Micro Raman spectra of (a) starting GONR and r-GONRs treated with CH_4-plasma with 5, 10, 15, and 30 minutes and (b) starting GONR and r-GONRs treated with H_2/CH_4-plasma with 5, 10, 15, and 30 minutes.

with varying treatment time. The Raman spectrum of the starting GONR reveals the D band, G band, 2D band, and, D + G band, at 1350 cm^{-1}, 1605 cm^{-1}, 2702 cm^{-1}, and 2925 cm^{-1}, respectively.[32] The prominent D peak is due to structural imperfections created by oxygen functional groups in the carbon basal plane[33,34] while the G-band is the so-called characteristic peak of graphite, corresponding to the sp^2 carbon bond stretching of E_{2g} mode.[33] The 2D band is the overtone of the D-band and typically used to indicate the quality of graphene films,[32,35] and the D + G band is attributed to the graphene lattice disorders.[36] After each of the various treatments by CH_4- and H_2/CH_4-plasmas with varying treatment time, it is found that the D band was slightly reduced while the 2D and D + G band were both increased. The decreased D band intensity and increased 2D band intensity suggest the sp^2 graphene domain size was increased in the as-treated r-GONR by plasma. We further estimate the layer numbers of as-treated r-GONR samples by analyzing the 2D bands in the Raman spectra.[32] According to the Raman result, it is suggested that the as-treated r-GONR samples are few-layered graphene structures with layer numbers in the range of 2 to 5.[32] The increased D + G band intensity is possibly due to the fact that the increasing of the sp^2 graphene domains in the as-treated r-GONR leads to an increase of disorders and domain boundaries. High temperature annealing should be helpful to reduced the D + G band intensity. Previous work suggests that the in-plane sp^2 crystallize size can be estimated from the ratio of the intensity of the D to G peaks (I_D/I_G),[37] and Fig. 6 shows the I_D/I_G of the as-treated r-GONR samples as a function of plasma treatment time. As the plasma treatment time was extended, the further decrease in I_D/I_G entailed increased reduction and fewer defects. The decline in defects was more substantial and effective following H_2/CH_4-plasma treatment compared with CH_4-plasma, which accords with our FTIR result (Fig. 2). We further noticed that the I_D/I_G of GONR were significantly reduced from 1.35 to 0.83 with 30 min H_2/CH_4-plasma treatment, suggesting that the H_2/CH_4-plasma treatment were not introduce additional defects into the r-GONR and quite effective on the reduction and defect repairing of GONR.

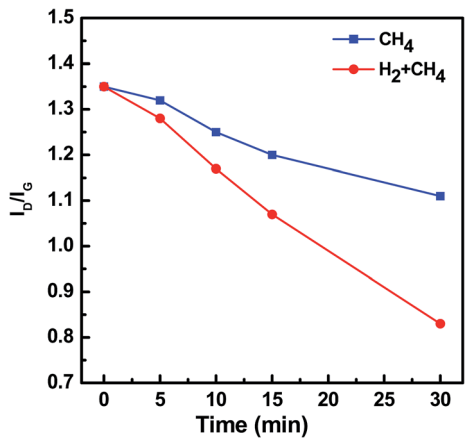

Fig. 6 Plot of I_D/I_G ratio estimated from the Raman spectra of GONRs treated with CH_4- and H_2/CH_4-plasmas as a function of plasma treatment time.

To reveal the relationship between the reduction level and the optical properties of as-treated r-GONR samples, the transmittance of thin film of r-GONR was measured and shown in Fig. 7(a). The Tauc's method was performed to estimate the optical bandgaps (E_g) of different r-GONR samples.[38] According to Tauc's formulation,[38] the E_g of GONR thin films can be derived from the plot of $(\alpha h\nu)^2$ *versus* $h\nu$, where α is absorption

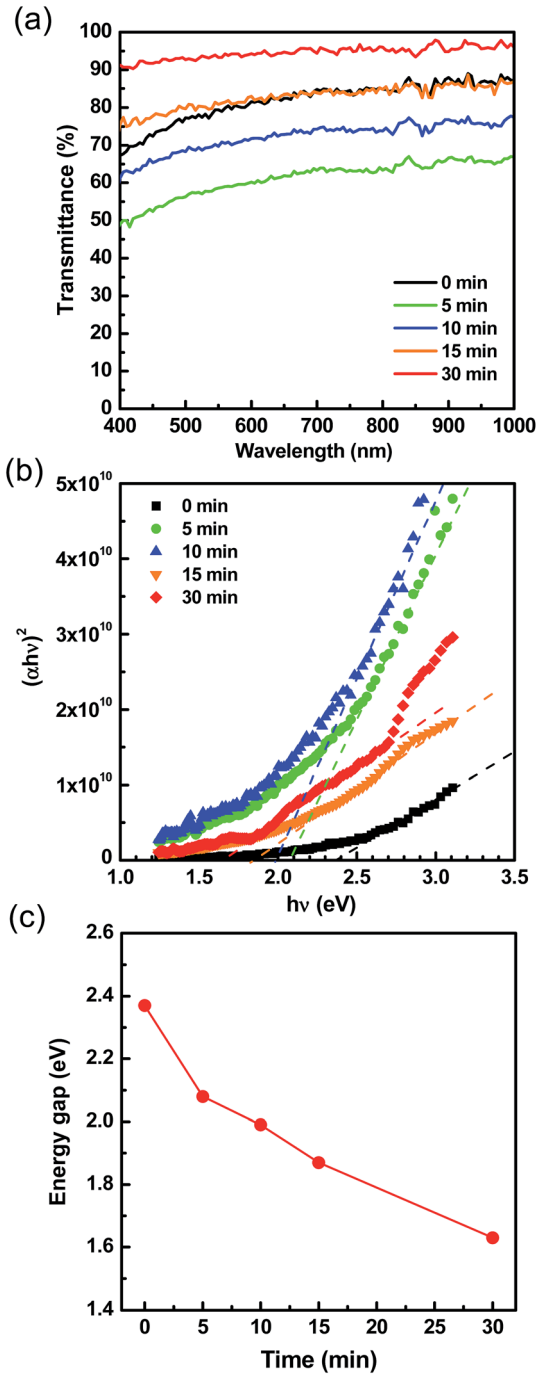

Fig. 7 (a) UV-Vis transmittance spectra of starting GONR, and r-GONRs treated by H_2/CH_4-plasma with 5, 10, 15, and 30 minutes. (b) Tauc's plot of starting GONR, and r-GONRs treated by H_2/CH_4-plasma with 5, 10, 15, and 30 minutes. (c) Plot of optical bandgap of GONR treated with H_2/CH_4-plasmas as a function of plasma treatment time.

coefficient, h is the Planck constant, and ν is frequency. The intersection point with the x-axis is the E_g. Fig. 7(b) and (c) show the resultant Tauc's plot and the plot of calculated E_g of as-treated r-GONR film as the function of the H_2/CH_4-plasma treatment time, respectively. The starting GONR exhibited an optical energy gap of 2.37 eV and, the E_g was decreased gradually with increased plasma treatment time. After 30 min H_2/CH_4-plasma treatment, the energy bandgap was reached 1.63 eV. This result suggests an intimate relationship between the optical bandgap and the reduction level of the r-GONR. The E_g of r-GONR can be tuned by simply controlling the plasma treatment time in our process. Theoretical and experiment evidence suggests the presence of an energy gap in GO and its direct dependence on the fraction of sp^2/sp^3 hybridized domains as well as the surface-functionalities. Initially, the insulating characteristics of GONR are well represented (2.37 eV, 0 min) due to the small sp^2/sp^3 ratio and high surface functionalities, according to the Raman (Fig. 5 and 6) and XPS result [Fig. 4(a)]. Within the first 5 min, a significant reduction is seen in the E_g (2.08 eV, 5 min). This result can be explained by the successful removing oxygen-containing groups indicated by the FTIR and XPS results and the sp^2 carbon domain repairing shown in the Raman analysis. Upon continuous plasma exposure for 10 min, the E_g progressively decreases to 1.99 eV. Over the next 20 min, a continuously decrease is seen in E_g, which is in conjunction with the XPS results that show a majority of the moieties being reduced during the same time frame. Upon removal of C=O and O–C=O species that have been found to decorate the edges of GONR sheets and are believed to be more difficult to remove,[31] according to the HRXPS analysis [Fig. 4(c) and (d)], the optical energy gap is seen to progress toward values that are generally less characteristic of insulators, and closer to those of semiconductors (1.63 eV, 30 min), which has not been reported for GONR reduction to our knowledge.

Electrical measurement was performed to further understand the effect of reduction level of r-GONR on their electrical properties. The passing current was measured by applying voltage to the two electrodes on the basal plate, which were coated with thin films of starting GONR and as-treated r-GONR by H_2/CH_4-plasma with varying treatment time. Ohm's law was employed to determine the sheet resistance and electrical conductivity of as-prepared r-GONR films. The sheet resistance equation used was $R_S = R \times W/L$, where R_S and R represent the sheet and electrical resistances, respectively, and W and L represent the width and length of the passage, and Ω square^{-1}

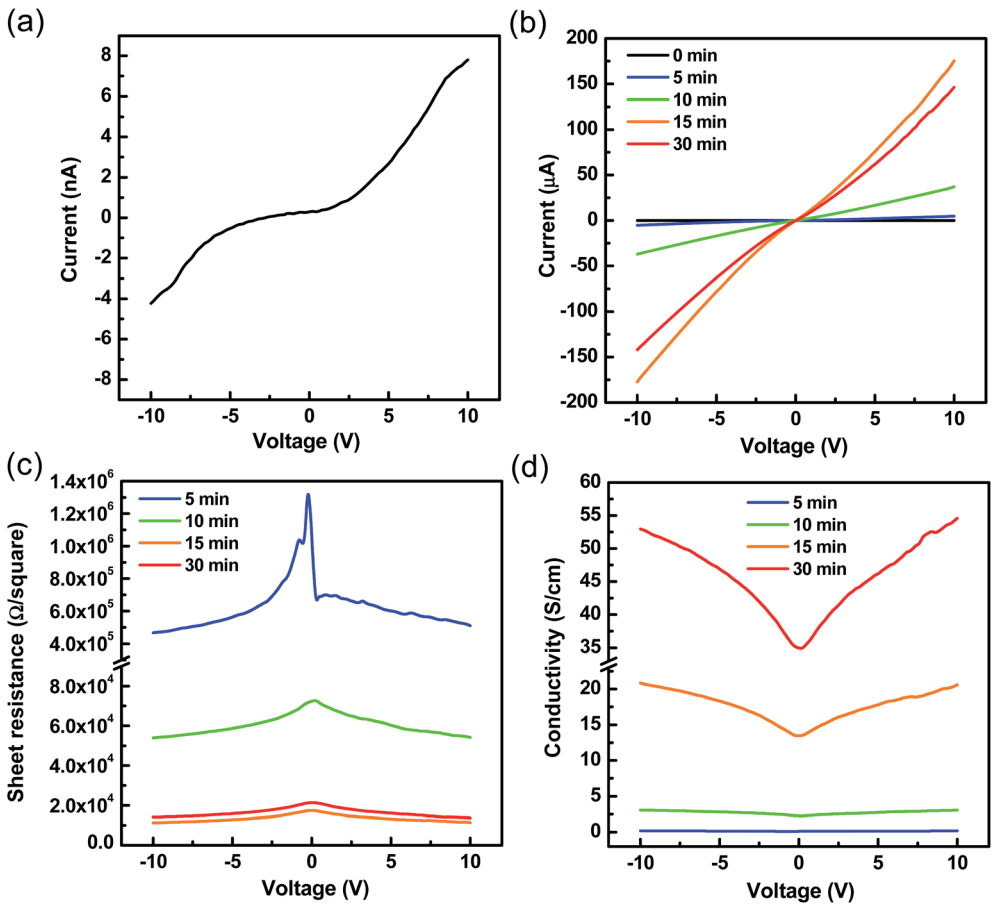

Fig. 8 (a) The I–V curve of starting GONR. (b) The I–V curves of GONR treated by H_2/CH_4-plasmas with varying treatment time. (c) The sheet resistance *versus* voltage of GONR treated by H_2/CH_4-plasmas with varying treatment time. (d) The conductivity *versus* voltage of GONR treated by H_2/CH_4-plasmas with varying treatment time.

is the unit of sheet resistance. For the electrical conductivity equation used was $\sigma = 1/R_S \times t$, where σ represents the electrical conductivity, t represents thickness, and the unit of electrical conductivity was (S cm^{-1}). Fig. 8(a) shows the non-linear relationship between the electrical current and voltage characteristics of the starting GONR, suggesting the electrical conductivity is at a relatively lower insulation state. Fig. 8(b) shows the results by comparing the electrical current and voltage characteristics of r-GONR treated by H_2/CH_4-plasma with varying treatment time. The data were more linear and indicate that the electrical current was enhanced from the original scale of nanoampere (nA) for starting GONR to the scale of ampere (A) of as-treated r-GONR, indicating that the electrical conductivity of r-GONR was improved after plasma reduction. The electrical current of the r-GONR treated by 30 min H_2/CH_4-plasma was slightly smaller than that of 15 min plasma treatment, and the reason could be due to the thinner film of r-GONR treated with 30 min. The measured sheet resistance [Fig. 8(c)] and the estimated electrical conductivity [Fig. 8(d)] of the r-GONR treated byH_2/CH_4-plasma with varying treatment time show that as the plasma processing time was increased, the sheet resistance and the electrical conductivity were decreased and increased, respectively. The improvement in the electrical conductivity is most probably due to a higher concentration of sp^2 graphene domains in the as-treated r-GONRs suggested from the FTIR and Raman characterizations (Fig. 2 and 4), which leads to enhanced electrical transport *via* percolation.[19] Overall, our optical and electrical measurements suggest an intimate relationship between the optical energy gap and the reduction level of the r-GONR, providing a method to tune the optical energy gap of r-GONR by simply controlling the plasma treatment time. It has been shown that reduction by hydrazine hydrate results in a higher I_D/I_G ratio that corresponds to a decrease in the sp^2 cluster size perhaps caused by the creation of defects, vacancies, or distortions of the sp^2 domains due to the removal of oxygen from the graphene sheets.[39,40] Our best sheet resistance ($\sim 1.5 \times 10^4$ Ω sq^{-1}; [Fig. 8(c)]) is comparable to the lowest reported value for hydrazine treatment, followed by thermal annealing ($\sim 4.3 \times 10^4$ Ω sq^{-1});[41] we note that our process is lower temperature and shorter exposure time. Further improvements in the conductivity may be possible by optimizing the exposure time, discharge current, and sample distance.

Conclusion

In summary, we have developed and studied a gas-phase, plasma-based process for the reduction of GONR. Simultaneously reduction and defect restoration of GONR was occurred during the H_2/CH_4 plasma treatment at low temperature of 240 °C. Our study shows that the synergistic effect of reduction and defect restoration makes it possible to engineer the optical energy gap and improve the electrical properties of GONR by controlling the H_2/CH_4 plasma exposure time. Overall, the plasma-based reduction of GONR demonstrated here open the possibility of low-temperature reducing GONR and GO for industrial-scale processing and applications.

Acknowledgements

This work was supported by the Ministry of Science and Technology of Taiwan (MOST Grant no. MOST 103-2221-E-011-150-MY2, MOST 104-2923-E-011-001-MY3, and MOST 103-2221-E-005-034), and was partially supported by National Taiwan University of Science and Technology (NTUST).

References

1 Y. W. Son, M. L. Cohen and S. G. Louie, *Nature*, 2007, **446**, 342.
2 C. Wang, Y. S. Li, J. J. Jiang and W. H. Chiang, *ACS Appl. Mater. Interfaces*, 2015, **7**, 17441–17449.
3 Y. Liu, X. Z. Wang, Y. F. Dong, Z. Y. Wang, Z. B. Zhao and J. S. Qiu, *J. Mater. Chem. A*, 2014, **2**, 16832–16835.
4 S. Wu, X. Q. Lan, F. F. Huang, Z. Z. Luo, H. X. Ju, C. G. Meng and C. Y. Duan, *Biosens. Bioelectron.*, 2012, **32**, 293–296.
5 N. S. Ismail, Q. H. le, H. Yoshikawa, M. Saito and E. Tamiya, *Electrochim. Acta*, 2014, **146**, 98–105.
6 E. F. Holby and C. D. Taylor, *Appl. Phys. Lett.*, 2012, **101**, 064102.
7 J. Lin, Z. W. Peng, C. S. Xiang, G. D. Ruan, Z. Yan, D. Natelson and J. M. Tour, *ACS Nano*, 2013, **7**, 6001–6006.
8 X. Wang, Y. Ouyang, X. Li, H. Wang, J. Guo and H. Dai, *Phys. Rev. Lett.*, 2008, **100**, 206803.
9 D. V. Kosynkin, A. L. Higginbotham, A. Sinitskii, J. R. Lomeda, A. Dimiev, B. K. Price and J. M. Tour, *Nature*, 2009, **458**, 872–875.
10 L. Y. Jiao, L. Zhang, X. R. Wang, G. Diankov and H. J. Dai, *Nature*, 2009, **458**, 877–880.
11 A. L. Elias, A. R. Botello-Mendez, D. Meneses-Rodriguez, V. J. Gonzalez, D. Ramirez-Gonzalez, L. Ci, E. Munoz-Sandoval, P. M. Ajayan, H. Terrones and M. Terrones, *Nano Lett.*, 2010, **10**, 366–372.
12 A. G. Cano-Marquez, F. J. Rodriguez-Macias, J. Campos-Delgado, C. G. Espinosa-Gonzalez, F. Tristan-Lopez, D. Ramirez-Gonzalez, D. A. Cullen, D. J. Smith, M. Terrones and Y. I. Vega-Cantu, *Nano Lett.*, 2009, **9**, 1527–1533.
13 L. Y. Jiao, X. R. Wang, G. Diankov, H. L. Wang and H. J. Dai, *Nat. Nanotechnol.*, 2010, **5**, 321–325.
14 L. Ma, J. L. Wang and F. Ding, *ChemPhysChem*, 2013, **14**, 47–54.
15 I. Jung, D. Dikin, S. Park, W. Cai, S. L. Mielke and R. S. Ruoff, *J. Phys. Chem. C*, 2008, **112**, 20264–20268.
16 S. Gilje, S. Han, M. Wang, K. L. Wang and R. B. Kaner, *Nano Lett.*, 2007, **7**, 3394–3398.
17 H. J. Shin, K. K. Kim, A. Benayad, S. M. Yoon, H. K. Park, I. S. Jung, M. H. Jin, H. K. Jeong, J. M. Kim, J. Y. Choi and Y. H. Lee, *Adv. Funct. Mater.*, 2009, **19**, 1987–1992.
18 C. Gomez-Navarro, R. T. Weitz, A. M. Bittner, M. Scolari, A. Mews, M. Burghard and K. Kern, *Nano Lett.*, 2007, **7**, 3499–3503.
19 C. Mattevi, G. Eda, S. Agnoli, S. Miller, K. A. Mkhoyan, O. Celik, D. Mostrogiovanni, G. Granozzi, E. Garfunkel and M. Chhowalla, *Adv. Funct. Mater.*, 2009, **19**, 2577–2583.

20 D. Yang, A. Velamakanni, G. Bozoklu, S. Park, M. Stoller, R. D. Piner, S. Stankovich, I. Jung, D. A. Field, C. A. Ventrice and R. S. Ruoff, *Carbon*, 2009, **47**, 145–152.
21 K. Ostrikov, E. C. Neyts and M. Meyyappan, *Adv. Phys.*, 2013, **62**, 113–224.
22 D. Teweldebrhan and A. A. Balandin, *Appl. Phys. Lett.*, 2009, **94**, 013101.
23 M. Cheng, R. Yang, L. C. Zhang, Z. W. Shi, W. Yang, D. M. Wang, G. B. Xie, D. X. Shi and G. Y. Zhang, *Carbon*, 2012, **50**, 2581–2587.
24 M. Baraket, S. G. Walton, Z. Wei, E. H. Lock, J. T. Robinson and P. Sheehan, *Carbon*, 2010, **48**, 3382–3390.
25 W.-H. Chiang, D. N. Futaba, M. Yumura and K. Hata, *Carbon*, 2011, **49**, 4368–4375.
26 D. V. Kosynkin, A. L. Higginbotham, A. Sinitskii, J. R. Lomeda, A. Dimiev, B. K. Price and J. M. Tour, *Nature*, 2009, **458**, 872–876.
27 A. L. Higginbotham, D. V. Kosynkin, A. Sinitskii, Z. Z. Sun and J. M. Tour, *ACS Nano*, 2010, **4**, 2059–2069.
28 S. Stankovich, R. D. Piner, S. T. Nguyen and R. S. Ruoff, *Carbon*, 2006, **44**, 3342–3347.
29 G. X. Wang, B. Wang, J. Park, J. Yang, X. P. Shen and J. Yao, *Carbon*, 2009, **47**, 68–72.
30 J. R. Rani, J. Lim, J. Oh, J. W. Kim, H. S. Shin, J. H. Kim, S. Lee and S. C. Jun, *J. Phys. Chem. C*, 2012, **116**, 19010–19017.
31 A. Bagri, C. Mattevi, M. Acik, Y. J. Chabal, M. Chhowalla and V. B. Shenoy, *Nat. Chem.*, 2010, **2**, 581–587.
32 A. Ferrari, J. Meyer, V. Scardaci, C. Casiraghi, M. Lazzeri, F. Mauri, S. Piscanec, D. Jiang, K. Novoselov and S. Roth, *Phys. Rev. Lett.*, 2006, **97**, 187401.
33 L. Malard, M. Pimenta, G. Dresselhaus and M. Dresselhaus, *Phys. Rep.*, 2009, **473**, 51–87.
34 A. C. Ferrari and J. Robertson, *Phys. Rev. B: Condens. Matter Mater. Phys.*, 2000, **61**, 14095–14107.
35 D. Graf, F. Molitor, K. Ensslin, C. Stampfer, A. Jungen, C. Hierold and L. Wirtz, *Nano Lett.*, 2007, **7**, 238–242.
36 M. A. Pimenta, G. Dresselhaus, M. S. Dresselhaus, L. G. Cancado, A. Jorio and R. Saito, *Phys. Chem. Chem. Phys.*, 2007, **9**, 1276–1291.
37 F. Tuinstra and J. L. Koenig, *J. Chem. Phys.*, 1970, **53**, 1126–1130.
38 J. Tauc, R. Grigorovici and A. Vancu, *Phys. Status Solidi B*, 1966, 627–637.
39 S. Stankovich, D. A. Dikin, R. D. Piner, K. A. Kohlhaas, A. Kleinhammes, Y. Jia, Y. Wu, S. T. Nguyen and R. S. Ruoff, *Carbon*, 2007, **45**, 1558–1565.
40 G. D. Yuan, W. J. Zhang, Y. Yang, Y. B. Tang, Y. Q. Li, J. X. Wang, X. M. Meng, Z. B. He, C. M. L. Wu, I. Bello, C. S. Lee and S. T. Lee, *Chem. Phys. Lett.*, 2009, **467**, 361–364.
41 G. Eda, G. Fanchini and M. Chhowalla, *Nat. Nanotechnol.*, 2008, **3**, 270–274.

